Ab initio calculation of charge transfer in proton collisions with N_2

E. Rozsályi,* L. F. Errea, L. Méndez, and I. Rabadán†

Laboratorio Asociado al CIEMAT de Física Atómica y Molecular en Plasmas de Fusión, Departamento de Química, Universidad Autónoma de Madrid, Madrid-28049, Spain

(Received 18 January 2012; published 2 April 2012)

Total and partial charge transfer cross sections are calculated in collisions of protons with the nitrogen molecule at energies between 0.1 and 10 keV. *Ab initio* potential energy curves and nonadiabatic couplings have been obtained for a number of N_2 bond lengths using a multireference configuration interaction method. The influence of the anisotropy of the target molecule is investigated. Results are compared with previous experimental and theoretical data.

DOI: 10.1103/PhysRevA.85.042701 PACS number(s): 34.70.+e, 34.10.+x

I. INTRODUCTION

Ion-molecule collisions are important events [1] in different environments including interstellar clouds [2], planetary atmospheres [3,4], comets [5], magnetic fusion reactors [6], and radiation damage of living tissues (see Ref. [7]). One of the important processes that take place in these events is charge transfer (CT), which leads to the ionization of the molecules and the possible production of fast neutrals. In this paper we concentrate on the study of proton collisions with nitrogen molecules, events that can occur in the polar regions of the Earth's atmosphere [8,9] due to the incoming flux of the solar wind, in which the typical energies of the protons are of the order of a few keV [10,11]. Proton collisions with N_2 may also be relevant in the edge of tokamak plasmas if N_2 is used as a scavenger, as suggested in Ref. [12].

The studies of $H^+ + N_2$ collisions in the energy region that goes from 100 eV to 10 keV are certainly not abundant. In the experimental side, we note the work of Birely [13], who measured the cross section of the CT process leading to the formation of $N_2^+(B\,^2\Sigma_u^+)$. Stier and Barnett [14] and Rudd *et al*. [15] measured CT total cross sections at energies above 5 keV, while Gao *et al*. [16] obtained integrated CT cross sections at 0.5, 1.5, and 5 keV. Luna *et al*. [17] measured the branching ratios of the dissociative and nondissociative channels contributing to CT and Quintana *et al*. [18] measured CT differential cross sections at energies between 0.5 and 3.0 keV, at scattering angles below 1°, showing that the dominant exit channel is $H(1s) + N_2^+(X\,^2\Sigma_g^+)$, although the energy-loss spectra displayed a secondary peak attributed in that work to the formation of $H(1s) + N_2^+(C\,^2\Sigma_u^+)$. On the theoretical side, we are only aware of the work of Cabrera-Trujillo *et al*. [19] at the three energies of Ref. [16]. At 5 keV, Gao *et al*. data are in good agreement with those of Stier and Barnett, but are 50% lower than Rudd *et al*. measurements and 40% higher than the theoretical data of Cabrera-Trujillo *et al*..

In this work we have applied a procedure similar to that employed in Ref. [20] for $H^+ + CH$ collisions. The calculation starts with a high-level *ab initio* calculation using MOLPRO [21] to obtain the potential energy surfaces of the first six electronic states of the supermolecule $(HN_2)^+$, and the corresponding nonadiabatic couplings between them. Some of these data are compared with Gianturco *et al*. [22], who performed an *ab initio* calculation of the N_2 and N_2^+ electronic states, and the $(HN_2)^+$ ion, although not in the same geometries that we employ in this work.

The accurate description of the target vibrorotational motion is particularly important as the collision energy decreases and the simple Franck-Condon (FC) approximation, where the target nuclei are fixed during the collision, becomes inappropriate. At not too low energies (above roughly 100 eV [23]), the sudden vibrational approximation [24], which involves a relatively modest computational effort, can be generally applied. In this vein, Dhuicq and Sidis [25] studied experimentally the vibrational excitation of N_2 in collisions with H^+, including electronic excitation and the CT mechanism, and concluded that the electronic transition is a sudden process with respect to the vibrational motion for collisional energies above 100 eV. Given the range of collisional energies of interest here, we apply the semiclassical eikonal approximation [26] and the vibrational sudden approximation to obtain the state-selected and CT cross sections using the SEIKON program [27].

In the following section we summarize the well-known semiclassical formalism and the vibrational sudden approximation employed. Then we give the molecular calculations details, and show the energies and dynamical couplings obtained. Cross sections are discussed in Sec. III. Atomic units are used unless otherwise stated, and the symbols a_0 and E_h are used to refer to the atomic units of length and energy, respectively.

II. COMPUTATIONAL METHOD

In the following equations we shall call $\boldsymbol{r}$ to the vector of the electron coordinates referred to the midpoint of the N_2 internuclear axis, $\boldsymbol{R}$ is the position vector of the proton with respect to the same origin, and $\boldsymbol{\rho}$ is the N-N internuclear vector (see Fig. 1). To describe the ion-molecule collision, we use the eikonal approximation [26], which is, in general, appropriate at the impact energies of the present work. In this approximation the projectile follows straight-line trajectories:

$$\boldsymbol{R} = \boldsymbol{b} + \boldsymbol{v}t \tag{1}$$

*Present address: Department of Theoretical Physics, University of Debrecen, P.O. Box 5, H-4010, Debrecen, Hungary.

†ismanuel.rabadan@uam.es

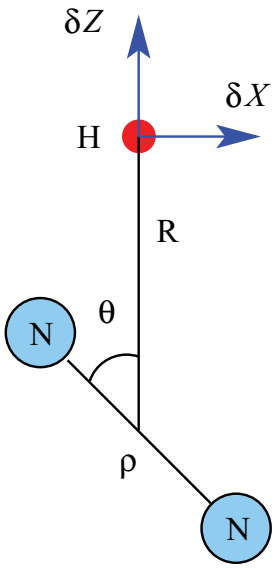

FIG. 1. (Color online) Internal nuclear coordinates and displacements used in the description of the $(HN_2)^+$ system.

with impact parameter $\boldsymbol{b}$ and velocity $\boldsymbol{v}$, while the electronic motion is described by a wave function $\Psi^{\rm EIK}$, solution of the eikonal equation:

$$H_{\rm int}\Psi^{\rm EIK} - i\left.\frac{d\Psi^{\rm EIK}}{dt}\right|_{\boldsymbol{r}} = 0. \tag{2}$$

The internal Hamiltonian has the form

$$H_{\rm int}(\boldsymbol{r},\boldsymbol{R},\boldsymbol{\rho}) = T_\rho + H_{\rm el}(\boldsymbol{r},\boldsymbol{R},\boldsymbol{\rho}), \tag{3}$$

where T_ρ is the kinetic energy operator for the nuclear motion of the target molecule and $H_{\rm el}$ is the Born-Oppenheimer electronic Hamiltonian of the three-center system:

$$H_{\rm el}(\boldsymbol{r},\boldsymbol{R},\boldsymbol{\rho}) = T_r + V(\boldsymbol{r},\boldsymbol{R},\boldsymbol{\rho}). \tag{4}$$

The eikonal-sudden approximation was explained in detail in [27]. Within this approach, the eikonal wave function is expressed as

$$\Psi^{\rm EIK}_{LM} = \rho^{-1}Y_{LM}(\hat{\boldsymbol{\rho}})\chi_0(\rho)D(\boldsymbol{r},t)\sum_j a_j(t;b,v,\boldsymbol{\rho})$$
$$\times\phi_j(\boldsymbol{r};\boldsymbol{\rho},\boldsymbol{R})\exp\left[-{\rm i}\int_0^t \epsilon_j dt'\right], \tag{5}$$

where χ_0 is the ground vibrational wave function of N_2 and $D(\boldsymbol{r},t)$ is a common translation factor (CTF) with the explicit form proposed in Ref. [28]. The collision wave function is expanded in terms of the molecular wave functions $\phi_j(\boldsymbol{r};\boldsymbol{\rho},\boldsymbol{R})$, eigenfunctions of $H_{\rm el}$ for the $(HN_2)^+$ system. Substitution of (5) into (2) leads to the system of differential equations:

$${\rm i}\frac{da_j}{dt} = \sum_l [\boldsymbol{v}\cdot\boldsymbol{M}_{jl} + v^2 B_{jl}]a_l \exp\left[-{\rm i}\int_0^t(\epsilon_l-\epsilon_j)dt'\right], \tag{6}$$

where $\boldsymbol{M}_{jl}$ are the nonadiabatic couplings, which include the correction terms due to the introduction of the CTF. The particular form of the translation factor also yields the couplings v^2B_{jl}, which are related to quadrupole matrix elements. The coupling terms $\boldsymbol{M}_{jl}$ and B_{jl} as well as the potential energy surfaces ϵ_j of Eq. (6) are functions of the internal nuclear coordinates R,θ, and ρ (see Fig. 1), and must be evaluated at each point of the projectile trajectory.

The cross sections for population of state f, $\sigma_f(v,\boldsymbol{\rho})$ are now obtained in eikonal calculations for each value of ρ:

$$\sigma_f(v,\boldsymbol{\rho}) = 2\pi\int_0^\infty bP_f(b,v,\boldsymbol{\rho})\,db\,, \tag{7}$$

where the probability P_f for transition to the final state ϕ_f is calculated from the coefficient a_f of expansion (5) obtained by solving (6):

$$P_f(b,v,\boldsymbol{\rho}) = \lim_{t\to\infty}|a_f(t;b,v,\boldsymbol{\rho}) - \delta_{if}|^2. \tag{8}$$

The orientation-dependent cross section in the sudden approximation is

$$\sigma_f^{\rm SV}(v,\hat{\boldsymbol{\rho}}) = \int_0^\infty \sigma_f(v,\boldsymbol{\rho})\chi_0^2(\rho)\,d\rho\,, \tag{9}$$

and the FC one is obtained simply by

$$\sigma_f^{\rm FC}(v,\hat{\boldsymbol{\rho}}) = \sigma_f(v,\boldsymbol{\rho}_e), \tag{10}$$

where ρ_e is the equilibrium distance of the diatomic target molecule.

The cross sections measured in beam-gas experiments correspond to the orientation average of those of Eq. (9) or, simpler, Eq. (10). The orientation average is equivalent to the sum over all values of the quantum number L of the initial wave function (5), assuming that all M values are equally probable [27]. This average can be performed in a similar way to the usual procedure of infinite order sudden approximation (IOSA) quantal treatments [29]. Within the semiclassical approximation, the dynamical calculations are carried out by assuming that the energies (ϵ_j) and couplings $(\boldsymbol{M}_{jl},\ B_{jl})$ of Eq. (6) only depend on the variable R, while θ and ρ are kept fixed as parameters (see Fig. 1). In this case, the integration of (6) leads to the coefficients $a_j^{\rm iso}(t;\rho,\theta,b,v)$ and, from them, to the isotropic transition probabilities $P_f^{\rm iso}(b,v;\rho,\theta)$ and cross sections $\sigma_f^{\rm iso}(v,\rho,\theta)$:

$$\sigma_f^{\rm iso}(v,\rho,\theta) = 2\pi\int_0^\infty bP_f^{\rm iso}(b,v;\rho,\theta)\,db. \tag{11}$$

By applying the vibrational sudden approximation of Eq. (9) and averaging over θ, we obtain

$$\bar{\sigma}_f^{\rm SV}(v) = \int_0^{\pi/2} d\theta\sin\theta\int_0^\infty \sigma_f^{\rm iso}(v,\rho,\theta)\chi_0^2(\rho)\,d\rho, \tag{12}$$

or the simpler FC orientation averaged cross section from Eq. (10):

$$\bar{\sigma}_f^{\rm FC}(v) = \int_0^{\pi/2} d\theta\sin\theta\,\sigma_f^{\rm iso}(v,\rho_e,\theta). \tag{13}$$

A detailed discussion on this θ averaging for $H^+ + H_2$ collisions can be found in Ref. [30], where it was pointed out that the orientation-averaged cross section $\bar{\sigma}(v)$ is very close to $\sigma_f^{\rm iso}(v;\theta)$ for θ in the range from 45° to 60°.

The coupling matrix elements of Eq. (6) can be expressed in Cartesian coordinates as

$$\boldsymbol{v}\cdot\boldsymbol{M}_{jl}(R;\rho,\theta)=\langle\phi_j|\,v_x\frac{\partial}{\partial X}\bigg|_{\rho,\theta}-v_z\frac{\partial}{\partial Z}\bigg|_{\rho,\theta}|\phi_l\rangle + \text{CTF correction terms}, \quad (14)$$

where the collision takes place in the XZ plane and $\hat{Z}=\hat{R}$.

A. Molecular calculations

Potential energy curves (PECs), nonadiabatic couplings, and quadrupole moments have been obtained, at all nuclear configurations, from multireference configuration interaction (MRCI) wave functions generated using the program MOLPRO and working within the Cs point group. In the following we detail the calculation steps.

We start with a Hartree-Fock self-consistent-field (HF-SCF) calculation of the $(H + N_2)^+$ singlet system to obtain an initial set of molecular orbitals. The basis set employed consists of $[4s,3p]$ contracted Gaussian type orbitals (CGTOs) plus a diffuse "s" [31] for H, designed to accurately reproduce the $n=1$ and $n=2$ levels of H, and the $[4s,3p,2d]$ CGTOs of Widmark *et al.* [32] for the N atoms.

The next step is the generation of the natural orbitals (NO) out of a complete-active-space self-consistent-field (CAS-SCF) calculation by defining a CAS consisting of 11 A' and 2 A'' orbitals, with the inner-shell A' orbitals corresponding to the $1s$ of the N atoms closed. NO are obtained by requesting six electronic states, all with the same weight in the CAS wave function.

A MRCI calculation using the NO produced in the previous step is performed to obtain the wave functions and eigenvalues. We have kept closed the two energetically lowest NO and we have included 7 A' and 2 A'' orbitals in the set of occupied orbitals. This gives around 5.3×10^5 contracted configurations (8×10^6 uncontracted ones) to build the MRCI wave functions corresponding to the first six singlet electronic states.

MRCI wave functions are obtained at slightly displaced nuclear positions in order to obtain the nonadiabatic couplings by a finite-difference method. In particular, in the initial geometry G, as illustrated in Fig. 1, we set the origin of coordinates in the center of mass of the nitrogen molecule, with the projectile H in the Z axis at a distance R and the nitrogen molecule bond at 45° from the Z axis in the XZ plane. The second geometry G_z is obtained by moving the projectile H along the Z axis to $R+\delta$, while the third geometry G_x is obtained displacing the projectile of G the amount δ in the X direction. Numerical stability in the calculation of the nonadiabatic couplings is obtained for values of $\delta\approx0.001\ a_0$ (see [33]). The nonadiabatic radial and rotational couplings are obtained by using $G-G_z$ and $G-G_x$ geometries, respectively.

Finally, quadrupole transition matrices are obtained for the G geometries using the MRCI wave functions.

B. Energies and couplings

The procedure described in the previous subsection has been repeated at N-N bond lengths from $\rho=2.0\,a_0$ to $\rho=2.2\ a_0$ in steps of $0.05\ a_0$. The PEC diagrams corresponding to three bond lengths, and for $\theta=45°$, are presented in Fig. 2. In those panels, the lowest curve correspond to the entrance channel $H^+ + N_2(X\,^1\Sigma_g^+)$, there are three CT channels (dashed lines), which dissociate into $H(1s)+N_2^+(X\,^2\Sigma_g^+)$, $H(1s)+N_2^+(A\,^2\Pi_u)$ and $H(1s)+N_2^+(B\,^2\Sigma_u^+)$ in the limit $R\to\infty$, and two target excitation channels (solid lines) $H^+ + N_2(a\,^1\Pi_g)$ and $H^+ + N_2(w\,^1\Delta_u)$. In the region between $R=2$ and $3\ a_0$, the upper curves show some kinks related to avoided crossings with lower Rydberg states of N_2^+. We have included experimental points (symbols) to mark the vertical excitation energies, at the N_2 equilibrium geometry, from the inferred PECs on the systems N_2 and N_2^+ constructed by Gilmore [34]. This asymptotic energy comparison is shown in Table I, where it can be seen that the computed energy differences are within 10% of the experimental ones. We also included in the table the excitation energies from the MRCI

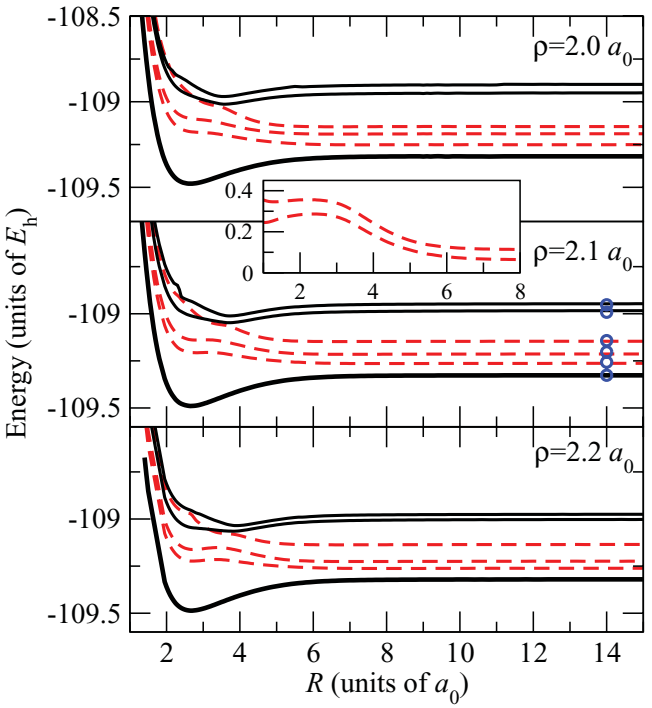

FIG. 2. (Color online) Potential energy curves obtained at $\theta=45°$ for several N-N bond distances as indicated in the panels. The solid lines correspond to $H^+ + N_2$ channels, while dashed lines are $H + N_2^+$ channels (see Table I). The symbols are obtained from the experimental excitation energies of [34]. The inset shows the energy differences E_2-E_1 and E_3-E_1 for $\rho=2.1\ a_0$.

TABLE I. Asymptotic energies (in Hartree) of the first five singlet electronic states of $(HN_2)^+$ relative to its ground state ($E_{gs}=-109.3267\ E_h$) at $\rho=2.1\ a_0$, and comparison with theoretical [22] and experimental data [34].

Channel	Present work	Theor. [22]	Expt. [34]
$H(1s)+N_2^+(X\,^2\Sigma_g^+)$	0.0635	0.0660	0.0698
$H(1s)+N_2^+(A\,^2\Pi_u)$	0.1132	0.1133	0.1249
$H(1s)+N_2^+(B\,^2\Sigma_u^+)$	0.1808	0.1838	0.1837
$H^+ + N_2(a\,^1\Pi_g)$	0.3432	0.3500	0.3344
$H^+ + N_2(w\,^1\Delta_u)$	0.3800	0.3707	0.3748

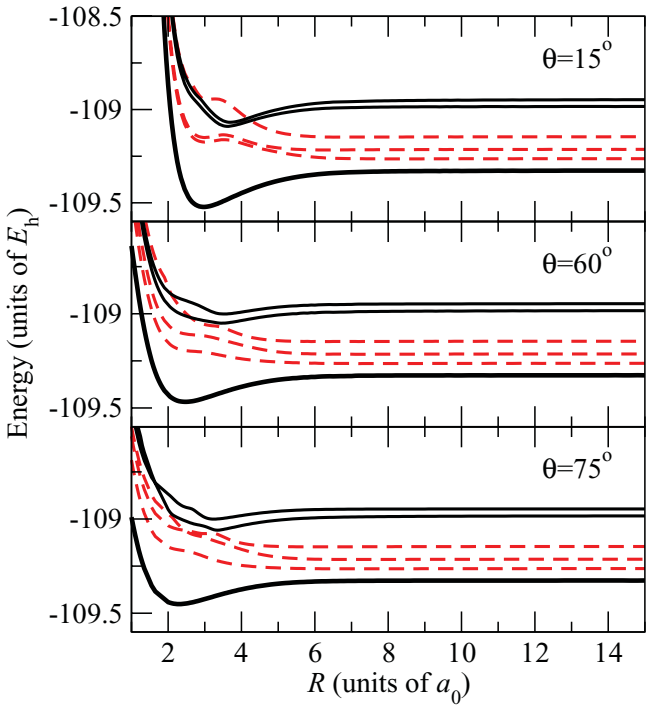

FIG. 3. (Color online) Same as in Fig. 2, with $\rho = 2.1\ a_0$ and θ values indicated in the panels.

calculation of Gianturco *et al*. [22], obtained from their Fig. 1 with the tool WebPlotDigitizer [35].

PECs at the N_2 equilibrium geometry ($\rho_e = 2.1\ a_0$), corresponding to three values of θ (15°, 60°, and 75°), are presented in Fig. 3. These sets of curves show that there are strong orientation effects in the PECs at projectile-target distances (R) below 3 a_0. These differences are bound to produce strong anisotropy effects in the cross sections dominated by transitions at low distances, but otherwise small effects are expected for transitions that take place at $R > 4\ a_0$.

In order to obtain the initial vibrational wave function χ_0, required to apply the sudden vibrational approximation, we have carried out a MRCI calculation for the ground electronic state of N_2, using the same CGTO basis set employed for the $(HN_2)^+$ system. The ensuing PEC is depicted in Fig. 4. We have obtained the vibrational wave functions and energies in this PEC using the program LEVEL [36], the probability densities of the first five states are included in Fig. 4, with indication on the lowest one of the five ρ values employed in the calculations.

A selection of the main nonadiabatic radial ($\partial/\partial Z$) and rotational ($\partial/\partial X$) couplings, corrected with v-terms translation factors, is shown in Fig. 5 as functions of R for $\rho = 2.1$ a_0 and $\theta = 45°$. One of the main features in these curves is the maximum in the radial coupling between states 1 and 2 that appears at $R \simeq 6\ a_0$, which is responsible for the largest contribution to the CT process.

In all sets of curves seen in Figs. 2 and 3, we notice that the entrance channel is below any exit channel, with the energies of the entrance channel and the CT channels running parallel as the projectile approaches the target. At $R \approx 6\ a_0$, the radial coupling between the entrance channel and the first CT one

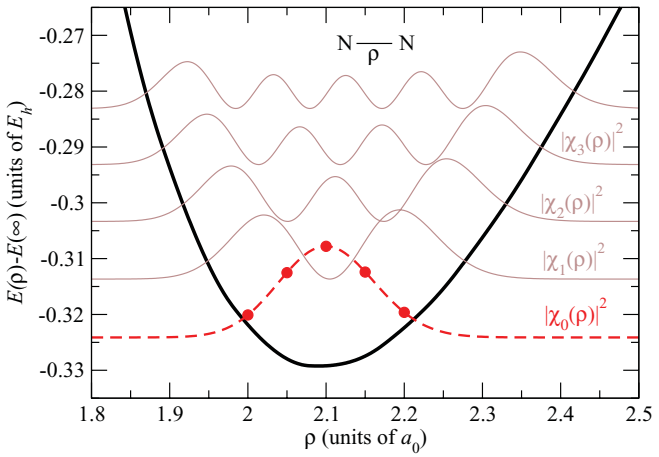

FIG. 4. (Color online) Potential energy curve of the electronic ground state of N_2 and the vibrational probability densities $|\chi_i|^2$ of the first five vibrational states. The bullets are displayed at the five values of ρ used in the vibrational sudden calculation of the CT cross sections.

develops a peak that is responsible for the main transitions at low energies between these states.

III. RESULTS

In Fig. 6 we show the opacity functions $bP^{\rm iso}_{1,j}$ as functions of b for the population of the three CT channels included in our calculation at three selected energies for $\theta = 45°$ and $\rho = \rho_e = 2.1\ a_0$. At $v = 0.5$ a.u., the three CT channels share the flux incoming from the entrance channel, while at

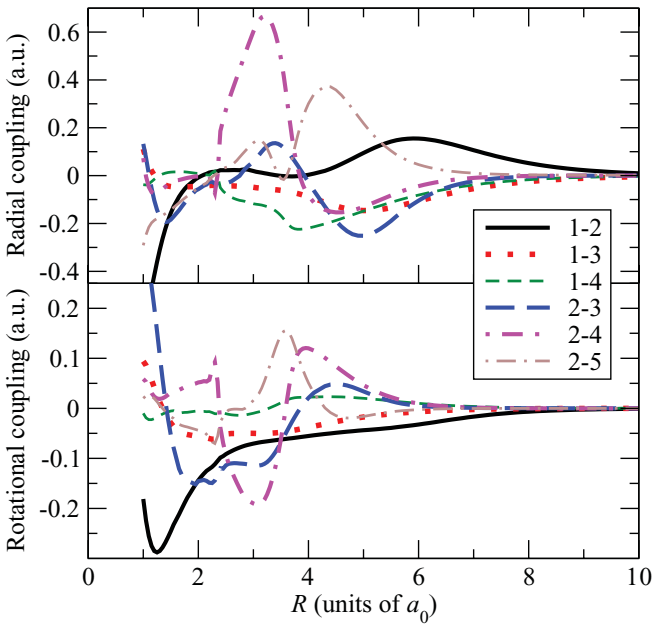

FIG. 5. (Color online) Radial $\langle\phi_i|\partial/\partial Z|\phi_j\rangle$ and rotational $\langle\phi_i|\partial/\partial X|\phi_j\rangle$ couplings corrected with v-terms translation factors in $H^+ + N_2(X\ ^1\Sigma_g^+)$ collisions along the projectile-target distance R and for a geometrical configuration given by $\rho = 2.1\ a_0$ and $\theta = 45°$ (see Fig. 1). The lines are labeled indicating ϕ_i-ϕ_j pairs of states, with the state number assigned in increasing energy order (see Table I).

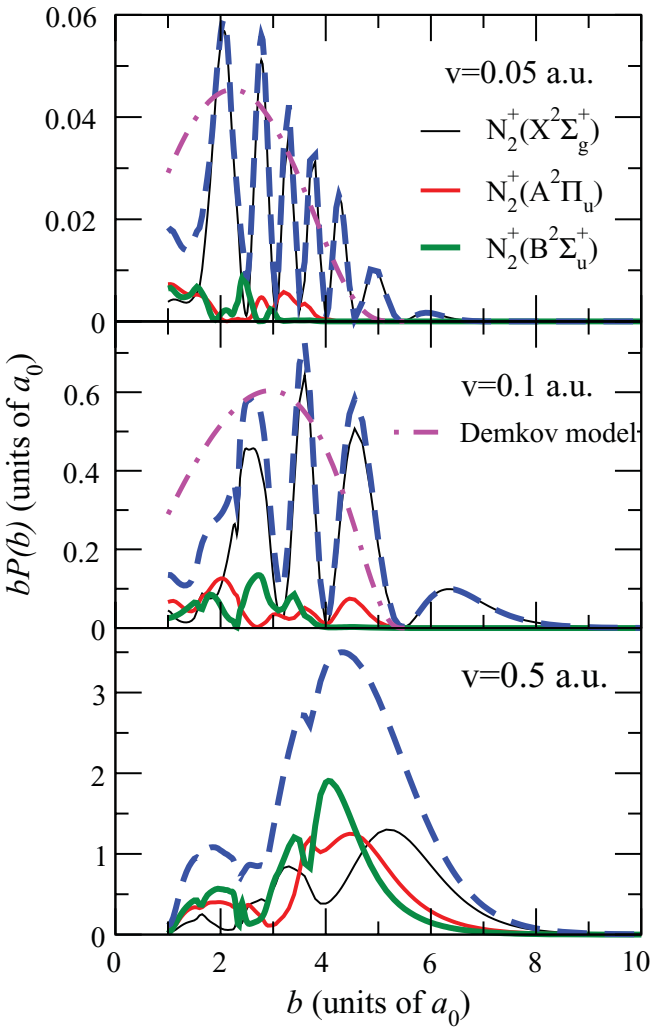

FIG. 6. (Color online) Opacity functions $bP^{\rm iso}_{1,j}(b,v;\ \rho = 2.1\ a_0, \theta = 45^\circ)$ for transitions to the first three CT channels (solid lines) at three impact velocities (indicated in the panels) in $H^+ + N_2(X\ ^1\Sigma_g^+)$ collisions. The dashed lines are the opacities for the total CT, and the dot-dashed lines are the nonoscillatory component of the probabilities obtained with the Demkov model [see Eq. (17)].

$v = 0.05$ and 0.1 a.u. the CT process is clearly dominated by transitions to $H(1s) + N_2^+(X\ ^2\Sigma_g^+)$. In these cases, the transition probabilities are qualitatively consistent with a Demkov model [37]. To obtain these curves we have diabatized the lowest two adiabatic states by integrating along R the radial coupling between them. This diabatization produces an interaction matrix element H_{12}, which has been fitted to an exponential function. For $\rho = 2.1\ a_0$ and $\theta = 45^\circ$ we obtain

$$H_{22} - H_{11} = \Delta H = 0.0635, \tag{15}$$

$$H_{12} = Ae^{-\lambda R} = -2.9\, e^{-0.82R}. \tag{16}$$

Following [38], the transition probability is

$$P = \mathrm{sech}^2\left(\frac{\pi \Delta H}{2\lambda v_r}\right) \times \text{oscillatory terms}, \tag{17}$$

where v_r is the radial velocity evaluated at the point where the adiabatic energy difference is equal to $\sqrt{2}(H_{22} - H_{11})$ (see, e.g., Ref. [39]).

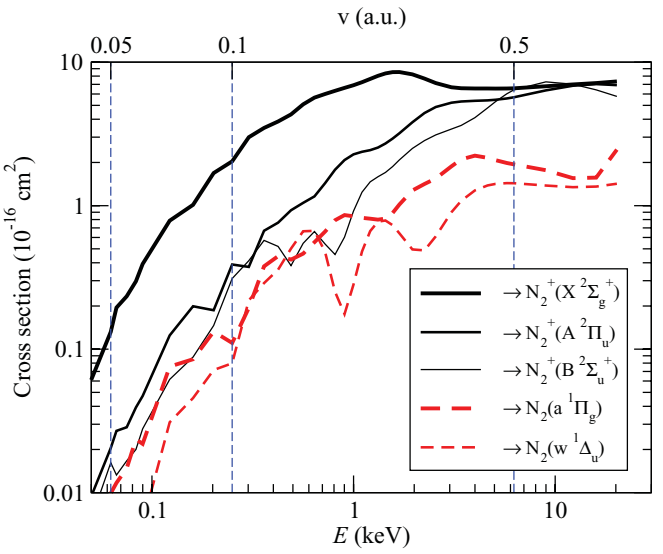

FIG. 7. (Color online) State-resolved CT cross sections $\sigma_f^{\rm iso}(v,\ \rho = 2.1\ a_0, \theta = 45^\circ)$ in $H^+ + N_2(X\ ^1\Sigma_g^+)$ collisions. CT channels are displayed as solid lines, while dashed lines correspond to excitation channels, as indicated in the figure.

We have included in Fig. 6 the nonoscillatory part of the Demkov probability of (17). The comparison with the close-coupling results shows that the two-state mechanism essentially reproduces the calculation at $v \leqslant 0.1$ a.u.; the differences are due to the rotational coupling. At $v = 0.5$ a.u., transitions to several excited states take place, as shown in Fig. 6; at this velocity a simple two-state model is not suitable, and the result of Eq. (17) is not shown.

Cross sections are obtained, according to Eq. (11), by integrating the functions of Fig. 6. Figure 7 presents the total state-resolved cross sections for both CT and excitation process in $H^+ + N_2(X\ ^1\Sigma_g^+)$ collisions. In the figure the three vertical lines mark the three impact energies at which $bP(b)$ functions are displayed in Fig. 6. Figure 7 indicates that transitions to $H(1s) + N_2^+(X\ ^2\Sigma_g^+)$ are dominant up to impact energies of about 2 keV. Above $E = 4$ keV, the three CT channels are competitive, while the excitation channels remain about 3 times smaller than CT ones.

In Fig. 8 we show the total CT cross sections obtained for the five fixed values of ρ considered in this work and the total vibrational sudden CT cross section of Eq. (9). In the same figure we have included the experimental results of Stier and Barnett [14], Rudd *et al.* [15], and Gao *et al.* [16], and the theoretical results of Cabrera-Trujillo *et al.* [19]. We note that the CT cross sections corresponding to various values of ρ show very similar shape and magnitude. The cross sections rapidly fall at low energies due to the relatively large energy gap (about 1.7 eV) the system has to overcome to populate the first CT channel. The FC CT cross section of Eq. (10) shows very little differences with the vibrational sudden one in the whole energy range studied. This is due to the linear behavior of the CT cross section as a function of ρ where the ground vibrational state of N_2 present significant probability density (see Fig. 4). One can also note that the different CT cross sections converge to the FC result as the energy increases, as expected. With respect to the comparison with the

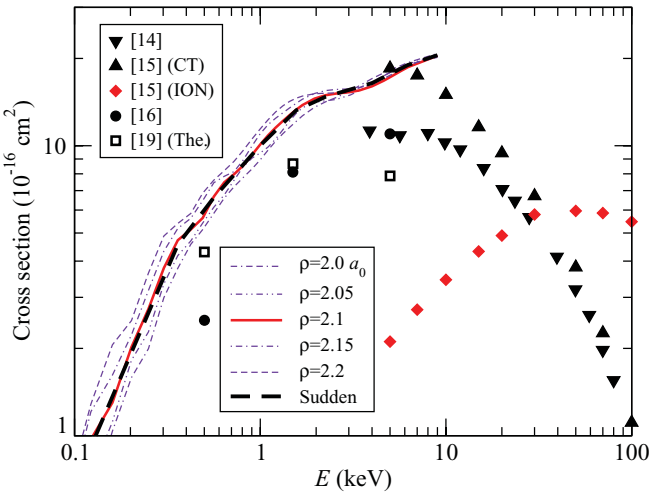

FIG. 8. (Color online) Total CT cross sections as functions of the impact energy in $H^+ + N_2(X\ ^1\Sigma_g^+)$ collisions. The lines are the present results with a fixed $\theta = 45^\circ$ for different values of ρ, indicated in the figure, and the vibrational-sudden result of Eq. (9). The solid symbols are experimental data of Stier and Barnett [14], Rudd *et al.* [15] (CT and ionization), and Gao *et al.* [16], while the empty symbols correspond to the calculations of Cabrera-Trujillo *et al.* [19].

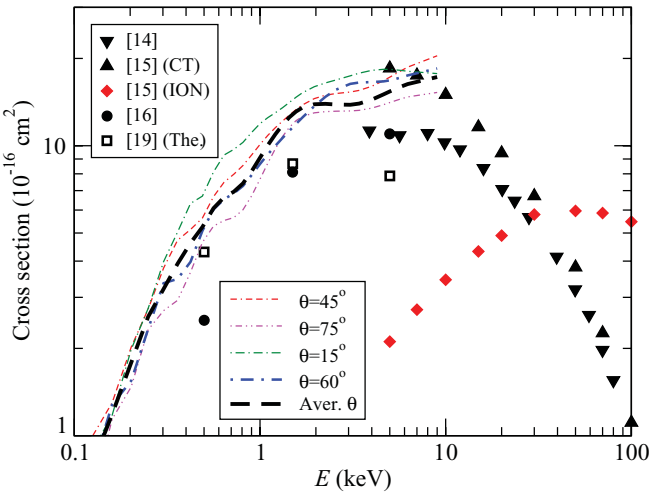

FIG. 9. (Color online) Same as Fig. 8 but, in this case, $\rho = 2.1$ a_0 and CT cross sections are presented for various values of θ, as indicated in the figure, along with the orientation-averaged one obtained with Eq. (13).

experimental data, although the shape of the cross sections is similar to those of Gao *et al.*, the magnitude is larger by a factor of 2. However, the magnitude of our cross section at $E \approx 5$ keV coincides with the results of Rudd *et al.* (with experimental uncertainty at this energy of 20%). In those experiments, it is assumed that two-electron processes are negligible, which is supported by the small (about 5%) transfer ionization cross section found by Luna *et al.* [17].

Due to the limited size of our close-coupling basis, we restrict the reliability of our CT cross sections to energies below 10 keV, where the ionization cross section is of the same order of magnitude as the CT one. In $H^+ + N_2$ collisions, experimental ionization and CT cross sections are identical at $E \approx 30$ keV, indicating that the populations of highly excited excitation and electron capture channels are probably not negligible for $E \gtrsim 20$ keV. The comparison of the present results with those of the calculation of Cabrera-Trujillo *et al.* [19] shows a large disagreement at $E = 5$ keV, while the agreement is better at $E = 0.5$ keV. This may be a consequence of the lack of flexibility of the single-determinant wave function employed in the method of Ref. [19] to describe transitions to excited states. In this respect, Cabrera-Trujillo *et al.* did not compare their results with the experiment of Rudd *et al.* [15], and attributed the low values of their total CT cross section with respect to that of Gao *et al.* [16] to the lack of ionization channels in their calculation. In our opinion, the relatively low value of the experimental ionization cross section (see Fig. 8) at $E \approx 5$ keV permits that a calculation that includes the relevant CT and excitation channels would yield reliable CT total cross section.

In Fig 8 we can also appreciate soft oscillations in our CT cross section as a function of impact energy. These oscillations are produced by interference effects originated by the avoided crossings between the PECs of the first and second CT channels with more excited ones around $R = 3$ a_0, which in turn lead to a maximum in their energy difference with respect to the entrance channel, as illustrated in the inset of Fig. 2.

To explore the influence of the projectile-target orientation in the magnitude and shape of the CT cross sections, we have performed calculations employing PECs (see Fig. 2) and dynamical couplings obtained at different values of θ for $\rho = \rho_e$, which yield (11). Figure 9 contains the total CT cross sections at four values of θ and the orientation-averaged cross section, from (13). As it can be seen, the general shape of the cross section does not change significantly with θ. This relatively small dependence of the CT cross section with θ is due to the large value of R where the main nonadiabatic transitions take place. At $R \approx 6$ a_0, the proton-N_2 interaction is almost isotropic (see Fig. 3). Nevertheless, the disagreement with the experimental data of Gao *et al.* remains similar as with the $\theta = 45^\circ$ of Fig. 8, and it is expected that an improved treatment of orientation effects during the collision as in Ref. [40] will not bring our results in agreement with those of Ref. [16].

IV. SUMMARY AND CONCLUSIONS

We have performed semiclassical sudden-vibrational eikonal calculations of state-selected cross sections for CT and excitation in $H^+ + N_2(X\ ^1\Sigma_g^+)$ collisions for impact energies between 0.1 and 10 keV. The potential energy curves and nonadiabatic couplings have been obtained by means of multireference configuration interaction calculations. The dynamical calculation include translation factor corrections. The electronic wave function is expressed as a linear combination of states of the supermolecule $(HN_2)^+$, which provides converged CT total cross sections for $E < 10$ keV.

We have found that the population of CT channels is dominated by transitions at $R \approx 6$ a_0, distances at which the potential energy curves are almost isotropic, which explains the relatively small influence of the target anisotropy in the CT cross sections. Furthermore, we have shown that, at low impact

energies (below 1 keV), the CT cross section is qualitatively well described by a simple two-state Demkov model. The population of excited CT and excitation states becomes sizable at energies higher than 1 keV. The total CT cross sections presented in this work are similar in shape to the experimental integrated data of Gao *et al*. [16], but they are about a factor of 2 higher in magnitude. We have checked that the influence of the N_2 vibration in the CT cross sections is negligible at the energies considered, and that the target anisotropy, while having a larger impact on the value of the CT cross section than the molecule vibration, does not explain the disagreement with Ref. [16]. However, our calculation shows good agreement with the experimental results of Rudd *et al*. [15] at $E = 5$ keV, which would suggest an underestimation of the total cross section in Ref. [16].

ACKNOWLEDGMENTS

This work has been supported by the Project ENE2007-62934 of the Ministerio de Ciencia e Innovación (Spain). Allocation of computational time at the CCC of the Universidad Autónoma de Madrid is gratefully acknowledged.

[1] M. E. Rudd, Y. K. Kim, D. H. Madison, and T. J. Gay, Rev. Mod. Phys. **64**, 441 (1992).
[2] S. Green, J. A. Montgomery, and P. Thaddeus, Astrophys. J. **193**, L89 (1974).
[3] J. F. Noxon, J. Geophys. Res. **75**, 1879 (1970).
[4] F. A. Gianturco, U. Gierz, and J. P. Toennies, J. Phys. B **14**, 667 (1981).
[5] S. Wyckoff and J. Theobald, Adv. Space Res. **9**, 157 (1989).
[6] P. Reinig, M. Zimmer, and F. Linder, At. Plasma Mater. Interaction Data Fusion **2**, 95 (1992).
[7] N. J. Mason, AIP Conf. Proc. **1080**, 3 (2008).
[8] M. Galand, D. Lummerzheim, A. W. Stephan, B. C. Bush, and S. Chakrabarti, J. Geophys. Res. **107**, A7 (2002).
[9] J. M. Ajello, R. S. Mangina, D. J. Strickland, and D. Dziczek, J. Geophys. Res. **116**, A00K03 (2011).
[10] E. Marsch, X.-Z. Ao, and C.-Y. Tu, J. Geophys. Res. **109**, A04102 (2004).
[11] E. Marsch, Living Rev. Sol. Phys. **3** (2006), [http://www.livingreviews.org/lrsp-2006-1].
[12] F. Tabares, V. Rohde, and the ASDEX Upgrade Team, Nucl. Fusion **45**, L27 (2005).
[13] J. H. Birely, Phys. Rev. A **10**, 550 (1974).
[14] P. M. Stier and C. F. Barnett, Phys. Rev. **103**, 896 (1956).
[15] M. E. Rudd, R. D. DuBois, L. H. Toburen, C. A. Ratcliffe, and T. V. Goffe, Phys. Rev. A **28**, 3244 (1983).
[16] R. S. Gao, L. K. Johnson, C. L. Hakes, K. A. Smith, and R. F. Stebbings, Phys. Rev. A **41**, 5929 (1990).
[17] H. Luna, M. Michael, M. B. Shah, R. E. Johnson, C. J. Latimer, and J. W. McCconkey, J. Geophys. Res. **108**, 5033 (2003).
[18] E. J. Quintana, V. R. Heckman, and E. Pollack, Phys. Rev. A **48**, 3670 (1993).
[19] R. Cabrera-Trujillo, Y. Öhrn, E. Deumens, J. R. Sabin, and B. G. Lindsay, Phys. Rev. A **66**, 042712 (2002).
[20] E. Bene, G. J. Halász, A. Vibók, L. F. Errea, L. Méndez, I. Rabadán, and M. C. Bacchus-Montabonel, Int. J. Quantum Chem. **111**, 487 (2011).
[21] H.-J. Werner, P. J. Knowles, G. Knizia, F. R. Manby, M. Schütz, P. Celani, T. Korona, R. Lindh, A. Mitrushenkov, G. Rauhut *et al*., *Molpro, version 2010.1, a package of ab initio programs* (2010), see [http://www.molpro.net].
[22] F. Gianturco, S. Kumar, and F. Schneider, Chem. Phys. **211**, 33 (1996).
[23] L. F. Errea, A. Macías, L. Méndez, I. Rabadán, and A. Riera, Phys. Rev. A **65**, 010701(R) (2001).
[24] V. Sidis, Adv. At. Mol. Phys **26**, 161 (1990).
[25] D. Dhuicq and V. Sidis, J. Phys. B **19**, 199 (1986).
[26] B. H. Bransden and M. H. C. McDowell, *Charge Exchange and the Theory of Ion-Atom Collisions* (Oxford University Press, Clarendon, 1992).
[27] L. F. Errea, J. D. Gorfinkiel, A. Macías, L. Méndez, and A. Riera, J. Phys. B **30**, 3855 (1997).
[28] L. F. Errea, L. Méndez, and A. Riera, J. Phys. B **15**, 101 (1982).
[29] M. Baer, G. Niedner-Schatteburg, and J. P. Toennies, J. Chem. Phys. **91**, 4169 (1989).
[30] L. F. Errea, A. Macías, L. Méndez, I. Rabadán, and A. Riera, Int. J. Mol. Sci. **3**, 142 (2002).
[31] See Supplemental Material at http://link.aps.org/supplemental/10.1103/PhysRevA.85.012702 for our basis for the hydrogen atom.
[32] P. O. Widmark, P. Malmqvist, and B. Roos, Theor. Chim. Acta **77**, 291 (1990).
[33] E. Bene, P. Martínez, G. J. Halsáz, A. Vibók, and M. C. Bacchus-Montabonel, Phys. Rev. A **80**, 012711 (2009).
[34] F. R. Gilmore, J. Quant. Spectrosc. Radiat. Transfer **5**, 369 (1965).
[35] A. Rohatgi, URL [http://arohatgi.info/WebPlotDigitizer].
[36] R. Leroy, Tech. Rep., University of Waterloo, Chemical Physics Research Report CP-661 (2005).
[37] Y. N. Demkov, Sov. Phys. JETP **18**, 138 (1964).
[38] E. E. Nikitin and S. Y. Umanskii, *Theory of Slow Atomic Collisions* (Springer, Berlin, 1984).
[39] P. Barragán, L. F. Errea, L. Méndez, and I. Rabadán, Phys. Rev. A **82**, 030701 (2010).
[40] P. M. M. Gabás, L. F. Errea, L. Méndez, and I. Rabadán, Phys. Rev. A **85**, 012702 (2012).